HAL
open science

Effect of cross-slot configuration in microfluidics on o/w emulsification at high throughput

Yongbin Ji, Jérôme Bellettre, Agnès Montillet, Patrizio Massoli

To cite this version:

Yongbin Ji, Jérôme Bellettre, Agnès Montillet, Patrizio Massoli. Effect of cross-slot configuration in microfluidics on o/w emulsification at high throughput. Microfluidics and Nanofluidics, 2021, 25 (10), pp.85. 10.1007/s10404-021-02486-z . hal-03351284

HAL Id: hal-03351284

https://hal.science/hal-03351284v1

Submitted on 22 Sep 2021

HAL is a multi-disciplinary open access archive for the deposit and dissemination of scientific research documents, whether they are published or not. The documents may come from teaching and research institutions in France or abroad, or from public or private research centers.

L'archive ouverte pluridisciplinaire **HAL**, est destinée au dépôt et à la diffusion de documents scientifiques de niveau recherche, publiés ou non, émanant des établissements d'enseignement et de recherche français ou étrangers, des laboratoires publics ou privés.

Effect of Cross-slot Configuration in Microfluidics on O/W Emulsification at High Throughput

Yongbin Ji [1], Jérôme Bellettre [1,*], Agnès Montillet [2], Patrizio Massoli [3]

[1] *LTeN UMR CNRS 6607, Université de Nantes, 1 rue Christian Pauc, CS 50609, 44306 Nantes Cedex 3,France*

[2] *GEPEA UMR CNRS 6144, Université de Nantes, 37 boulevard de l'Université, BP 406, 44602 Saint Nazaire, France*

[3] *Institute of Sciences and Technologies for Sustainable Energy and Mobility (STEMS) - CNR, Viale Marconi 4, 80125Napoli, Italy*

[*] ***Corresponding author: jerome.bellettre@univ-nantes.fr***

Abstract

The Liquid-liquid dispersion process is experimentally investigated to manufacture oil-in-water emulsion working at high flowrates in the cross-slot type of microfluidics. Two cross layouts, namely symmetric and asymmetric configurations, are compared via characterizing the droplet size and size distribution. Automated granulometry is implemented on the images taken by microscopy observations of the emulsion samples. High-speed shadow photography is carried out to discover the continuous and dispersed phase flow interactions in the vicinity of the collision region. The results show that the designed microsystems present great potential in terms of fabricating fine oil droplets distributed in the final emulsion. The arithmetic averaged diameter is less than 10 ***μm*** at all tested flow conditions and the minimum mean diameter reaches 3.9 ***μm*** at the highest energy consumption case. Because of the higher shear stress and more intensified interaction, the symmetric geometry of the cross-slot is beneficial to create fewer amounts of large droplets and dispersing the oil phase more uniformly at the same hydrodynamic conditions, especially in the low Reynolds flow case in this study. As the flowrate is enhanced, the disparity between them is diminished attributed to the instability inside the channel reaches a high level. The mean drop diameter for both systems is capable to be scaled with the emulsion velocity based Weber number. The detrimental effect of the symmetric configuration is that the energy required to burst the dispersed streams is relatively a little higher than with asymmetric one.

Keywords: O/W emulsification; microchannel; two-phase flow; high throughput; swirl

Nomenclature

D	diameter of the droplet, *μm*
D_{10}	arithmetic mean diameter, *μm*
D_{32}	Sauter mean diameter, *μm*
D_{h_d}	hydrodynamic diameter of dispersed channel, *μm*
D_{max}	maximum droplet diameter, *μm*
f	oil to water volume ratio,-
$\dot{m}$	mass flow rate, *kg/s*
p_L	Laplace pressure, *bar*
P	pressure, *bar*
R	radius of the droplet, *μm*
S_p	specific surface area, μm^{-1}
$\dot{V}$	volume flow rate, *mL/min*
U	superficial velocity, *m/s*

Greeks

γ	surface tension, *mN/m*
δ	standard deviation, -
μ	dynamic viscosity, *mPa·s*
υ	kinematic viscosity, m^2/s
ρ	density, kg/m^3
σ	interfacial tension, *mN/m*
φ_d	oil volume fraction in the emulsion, *mN/m*
τ_s	shear stress, *bar*

Subscripts

c	continuous phase (water)
d	dispersed phase (oil)

e emulsion

Acronyms

Ca Capillary number,-
c.d.f Cumulative distribution function, -
p.d.f Probability distribution function, -
PdI polydispersity index,-
Re Reynolds number,-
We Weber number,-

1. Introduction

The emulsion is a common system of dispersing one fluid into another one via different emulsification methods. It is ubiquitous to our daily life science and has been widely utilized in various industries, for example, drug delivery for pharmaceutical application (Lawrence and Rees 2000), food processing (Galus and Kadzińska 2015), refining of petroleum and its transportation in energy engineering (Kilpatrick 2012), and so on. In an emulsion-based product, particle size and size distribution contribute to the physical appearance, stability and rheological properties of the finished products. More specifically, they control flocculation (droplet diffusion in continuous phase), coalescence, resistance to sedimentation or creaming. As a rule of thumb, fabrication of more homogeneous emulsion with finer dispersed droplets inside is one of the most paramount goals for developing various emulsification devices. The drop size and size distribution are highly dependent on the working mechanism of the facilities, which is further related to the imposed hydrodynamic condition, the configuration of the emulsifier as well as the physical and interfacial properties of the two-phase liquids.

Rayleigh (1878) firstly studied the conditions governing the breaking up of a jet of one fluid projected into another, showing the effect of surface tension in making cylindrical liquid thread unstable and breaking into drops further. Taylor (1932) addressed the mechanism of emulsion formation in the viscous flow and pointed out that the balance of the external disruptive force and the internal cohesive force determines the breakage of the dispersed liquids as well as the final droplet size. At low Re flow conditions, the velocity gradient induced shear stress, τ_s, acts as the destructive force, and the interfacial resistance force, representing as Laplace pressure ($p_L = 2\sigma/R$), developed across the interface between two fluids prevents the dispersed phase to be fragmented. However, the dominant disruptive stress in the turbulent flow for emulsification changes to be the dynamic pressure fluctuation inside the flow field resulting from the unstable velocity (Kolmogorov 1949; Davies 1985).

Great amounts of work have been carried out to study different methods for emulsification, including agitating the mixture of two-phase liquids in a tank using impellers (Chen and Middleman 1967; Solsvik and Jakobsen 2015), static mixers (Lemenand et al. 2003; Theron and Sauze 2011), high-pressure homogenizers (Paquin 1999; Schlender et al. 2015) and low or high-frequency ultrasonic generators (Abismail et al. 1999; Taha et al. 2020). Apart from these relatively mature techniques, other new concepts of liquid-liquid dispersion systems are continuously proposed to improve the mixing intensity. For example, Habchi et al. (2009) and Lemenand et al. (2014) investigated oil and water mixing by chaotic advection in a specially designed twisted-pipe flow for generating o/w emulsions. They pointed out that, attributed to the secondary flow inside the helical pipe, shear stress for disrupting oil streams gets enhanced greatly, which further leads to the finer and more mono-dispersed droplets. Luo et al. (2017) also demonstrated the performance of this kind of helical tube reactor in terms of manufacturing a stable water-organic solvent dispersion by characterizing the mean drop diameter and its correlation with energy dissipation rate.

The merit of the above-mentioned emulsification methodologies lies in their usage of greater kinetic energy at high-throughput. Thus, the production efficiency is higher but the droplet size is difficult to be well controlled. Microfluidics, attracting plenty of focus in recent decades, is another essential technical pathway to handle two-phase liquids dispersion issues. Basically, it is a droplet-based technology and well known for its superiority in manipulating droplet dimensions, so that the created emulsion from the microfluidics is closer to a mono-dispersed system (Zhao and Middelberg 2011; Moreira et al. 2021). Three conventional types of configurations, namely, flow focusing (Anna et al. 2003; Cohen et al. 2014), cross flowing (Y or T junctions) (Thorsen et al. 2001; Ushikubo et al. 2014), and co-flowing (Cramer et al. 2004; Perro et al. 2011), are most widely applied and studied. Normally, the flow rate imposed in these microfluidic devices is limited ($\mu L/min$), which constrains the hydrodynamic flow conditions in the microchannels to be in the low Re regime. The match of Capillary number

of continuous and dispersed flows (Ca_c and Ca_d) corresponds to five breakage mechanisms or modes: squeezing, dripping, jetting, tip streaming, and tip-multi-breaking (Zhu and Wang 2017). The final droplet size and distribution is associated with the flow conditions and geometric parameters for every category of the microsystem. Straight-through microchannels (Kobayashi et al. 2008) or membrane emulsifiers (Nakashima and Shimizu 1988; Vladisavljević GT 2012) are also developed, which can be viewed as the parallel arrangement of microchannels by adopting porous structures.

Considering the fact that the possible flow rate can be treated in these microfluidic facilities is far away from the demand of industrial applications, Belkadi et al. (2016) proposed the cross-junction microchannel model to fabricate emulsified biofuel by impinging continuous and dispersed phase fluids directly. It is designed to work at flow rates two or three orders of magnitudes (mL/min) higher than with the traditional microfluidic device. In fact, the head-on impinging configuration in mini or micro-channels has been utilized broadly for miscible fluids mixing, known as micro-mixers, showing significant advantages of efficient mixing (Mahajan and Kirwan 1996; Ait Mouheb et al. 2011; Bothe et al. 2006; You et al. 2017). Applying two-impinging-streams to emulsify is firstly reported by Tamir and Sobhi (1985). They injected streams of the kerosene-water mixture (coarse oil-in-water emulsion) via spray guns in a face-to-face collision layout to obtain the final finer emulsion. Comparisons between this stream-impinging system and homogenizer indicated that the new two-impinging-streams device performs better in terms of producing droplets finer and narrow-distributed droplets. Kiljański (2004) experimentally investigated the effect of the distance between two injectors in the setup of the Tamir's device on the dispersion process and outcome. They found that there is an optimum gap at which the best disintegration of drops would be realized. These reviewed works inspire the idea of impinging two-immiscible liquid jets in a microchannel for emulsion generation; mainly taking advantage of transporting and dissipating the higher kinetic energy into the confined collision area. Siddiqui and Norton (2012) and Siddiqui (2014) performed investigations on confined impinging jets mixer for oil-in-water emulsification working at high-throughput. The tested Reynolds number reached as high as 13000. By characterizing the droplet size and its distribution, it was shown that the mean drop diameter is highly dependent on jet Reynolds number or energy dissipation rate. Tsaoulidis and Angeli (2017) experimentally examined water-oil dispersion in a similar opposed-jets collision configuration at varied hydrodynamic and geometric parameters. It is concluded from their results that the sum of two jets velocity influences the drop size and interfacial area most.

To sum up, the literature points out that most efforts have been made on measuring the droplet size and revealing breakage mechanism of two liquids dispersion in the conventional microchannels. But studies on the oil in water emulsification via cross-slot impinging configuration, especially working at high throughput, are relatively rare. This work is aimed to characterize droplet size and size distribution in cross-slot microsystems employing head-on impingement of oil and water jets for emulsifying. The flow rate imposed is at *mL/min* level, which is much higher than most of those implemented in microfluidics. Except for the hydrodynamic conditions, the effect of the cross-junction layout on the emulsion quality is the main focus of the present study. As a complementary part of this work, flow visualizations in the microfluidics is also carried out to disclose the two-phase fluids interaction at different flow conditions in two configurations.

2. Methodology

2.1 Experimental setup

The experimental test bench used to obtain oil-in-water (o/w) emulsion with the studied microfluidic devices is outlined in Fig.1. The continuous phase (water) and dispersed phase (rapeseed oil) are supplied into the device by two Armen pumps (AP TRIX 500). Fluid at a flow rate up to 500 mL/min is possible in the microsystems thanks to these pumps as their working pressure can reach up to 200 bar. Two weighing scales (Sartorius-MSE 2203) with an accuracy of 0.001 g are used to measure flowrates of water ($\dot{m}_c$) and oil ($\dot{m}_d$). To assess the pressure drop through the microchannels, two Gems 31IS series pressure transducers (0-250 bar) with an accuracy of 0.25% are assembled at the inlet channels for both phases. The measurements of flow rate and static pressure are synchronized by connecting to a NI DAQ module (USB-6009 analog to digital). All connection pipes between the pumps and microchannel are Fluoropolymer tubing with an inner diameter of 1.55 mm. The emulsion issues from outlets at atmospheric pressure condition and then is collected in a container to perform sampling microscopy analysis.

2.2 Microchannels

The microsystem designed for highly efficient oil-in-water emulsification utilizing the impingement configuration of two streams is shown in Fig.2; one of them, depicted in Fig.2(b), has been investigated previously by Belkadi et al. (2016) for the emulsified biofuel (water-in-oil emulsion) production. Fig.2(a) depicts the general 3D layout of the devices. Each microsystem is composed of two PMMA plates. For the asymmetric system, the channels and a groove for a seal are (mechanically) etched into one of the plates (bottom plate). The sealing of the system is ensured by a gasket and closing the system with nuts and screws. The thickness of the plates and the positioning of the screws are studied in order to prevent the deformation of the plates under the effect of the pressure. The symmetrical system, as indicated in the manuscript, is more complex because the two plates are engraved. Due to their design, each system can be opened for maintenance, if necessary, but usually cleaning in place is sufficient to preserve it. The tubes are inserted on a commercial connector, a flat-bottomed fitting, which is screwed on a threaded hole made in the upper PMMA plate. A ferrule is used to ensure a tight seal. The details of the microchannels layout and dimensions are shown in Fig.2(b) and Fig.2(c). Water and oil streams develop in the feeding channels (in the X direction) and form a head-on impingement to strengthen the interactions and breakup. The water channel and emulsion outlet channels have the same square cross-section dimensions, which is 600 $\mu m \times 600\ \mu m$. Recognizing the dispersed phase fraction is normally not exceeding 20-30% for most emulsification applications, the flow rate of the dispersed phase flow is usually several times smaller than the continuous phase. In order to enhance the further impact intensity between the two phases and disperse oil streams into the final emulsion as finer droplets consequently, the inlet channel size for the dispersed phase transportation is designed to be only half of that for the continuous phase, that is, 300 $\mu m \times 300\ \mu m$. This dimensional inequality of the two inlet channels naturally leads to the possibility of designing different cross-slot geometric layout plans. Therefore, based on the relative positions in the YZ plane for the two inlet axes, two configurations will be compared here; they are respectively designated as, asymmetric and symmetric. The asymmetric configuration (Fig.2(b)) is characterized by an offset of water and oil feeding channels axis in the depth direction (Z) with a magnitude of 150 μm. As mentioned, it has previously been investigated. It has to be emphasized that there is no off-axis in the Y direction to ensure two emulsion outlets still symmetrical. As for the symmetric one (Fig.2(c)), oil and water channels are simply coaxial by grooving the same "half-depth" channels on both slabs. Overall, the water and oil channels are in the X direction with a total length of 20 mm respectively. The emulsion outlet channels also have a length of 20 mm. Generated emulsion flows firstly towards along the two opposite Y directions. Then, 90° bends in a middle way turn it to flow following the negative X direction, as illustrated in Fig.2(d). These bends are intended to enhance the breaking-up of droplets (Belkadi et al. 2018). It has to be noted that previous works have led to the current design of the asymmetric system. For example, the effect of the number of bends (Bellettre et al. 2017) and the length of the outlet channels (Belkadi et al. 2018) have been studied. It has been observed that the length of the outlet channels should be selected depending on the viscosity ratio of the fluids. For the vegetable oil like sunflower oil and water, a length of 20 mm is beneficial, while for the couple of gasoil/water using a shorter length (10 mm) should be preferred. This is correlated to the flow pattern developed inside the outlet channels. Dispersion of or within a viscous fluid needs a longer length to make efficient the break up mechanisms. The presence of a bend has been shown to be beneficial compared to a straight outlet channel, but incrementing the number of bends from one to six has shown that it does not help to improve the break-up. For sure, the role of singularities remains to be explored more thoroughly, in particular the spectrum of possible geometric changes is still wide.

Fig.2(e) presents the XZ section plane of the two systems with imposed velocity profiles. The important feature of asymmetric configuration is that swirl flow structure can be formed in the impingement zone due to the offset axis arrangement for the two impinging channels. The effect of this macro swirl flow in the asymmetric configuration on the two-phase flow patterns in the vicinity of the impact area and single drop breakage behavior has been recently specifically studied (Ji et al. 2020; 2021). The results indicate that the swirl flow can promote emulsion quality, that is, finer and less poly-dispersed droplets, especially at high Re conditions. Also, the swirl flow resulting in low-pressure center favors drops to be trapped into it, and thus the kinetic energy is efficiently dissipated for fragmenting. Concerning the symmetric configuration, which is investigated for the first time in this contribution, the oil jet penetrates into the facing water streams. Velocity gradient in the shear layers where two-phase flows contact could also induce a counter-rotating swirl pair. The comparison of the two cross-slot configurations in terms of fragmenting the dispersed phase is the main purpose of the present study.

2.3 Droplet size measurement & automated granulometry

The size of oil droplets is measured in the o/w emulsion sample collected from the container, this one receiving emulsion from both outlet microchannels (shown in Fig.1). There is no significant difference between the emulsions from the two outlets in terms of droplet statistical results since it has been verified that the flow patterns are similar in each outlet channel. Thus, the collected testing sample from the container can be viewed as a comprehensive result of the final emulsion from the two outlet channels. An Olympus upright optical microscope is utilized with assembling 5× and 50× objective lens chosen case by case. The high-resolution image shoot by the microscope is then analyzed by a granulometry code in Matlab. The characteristic dimension of dispersed drops is obtained from a sample of a sufficient number of droplets, taking into account the statistical size dispersion as explained hereafter. One typical example of the microscopy image can be seen in Fig.3. The left one is observed with the lower magnification objective lens (5×), which gives an overall view of how oil droplets distribute inside an emulsion sample drop. Zoomed-in images with higher magnification (50×) at two regions respectively, A and B, are presented also. Some heterogeneities in size distribution from an area to another one make that it is necessary to consider a high number of droplets. Indeed, if only droplets picked up near region A or B are analyzed and even if the convergence of the drop mean diameter is obtained, it can't represent the comprehensive situation and reflect true averaged drop size as well as size distribution. To avoid the problem, we carry out the measurements according to the following steps. Firstly, the emulsion is collected after a stable emulsification process reached at each testing condition, and a dilution of the emulsion proceeds with a factor of 10 in the continuous aqueous phase. Then only one sample emulsion drop is dripped by syringe on the microscopy slide. Normally, the area of emulsion drop spreading on the glass slide is roughly 2mm*2mm. Then, a 5× objective lens is utilized to get a full image of the sample drop and anchoring its XY locations in the microscope system. Lastly, the highest magnification accessible (50×) is switched to scan the measured emulsion drop from the left-top edge of the drop to the right-bottom one. At this magnification, the spatial resolution is 0.068 μm/pixel. Meanwhile, snapshots are taken and recorded. In this way, all the oil droplets in the sample emulsion drop are captured and statistically analyzed from nearly 100 images, and around 5000 droplets in total will be identified correspondingly.

Acquired images are processed via in-house automated granulometry coding by Matlab. The procedure for microscopy images analysis is shown in Fig.4. The original image is converted to the gray image in the first step. The contrast of the image is then enhanced to make the oil-water interface clearer for binarization. In the binarized image, the edges of the oil droplets are kept. Border clearing to avoid the mistake of considering two bonded droplets as one and holes filling are performed consecutively. Finally, the distributed regions marked as white dots are identified as the final droplets and their region properties are then extracted. What has to be mentioned, from a previous work performed using the asymmetric microsystem and based on laser diffraction particle size analysis, is that droplets with a diameter less than 1μm are statically much less frequent in the obtained emulsions. So the lower cutting threshold is set to escape from counting noise on the images. After all-drops information is obtained from image sequences, statistical analysis of drop size and size distribution is performed.

From the statistical analysis of droplet diameter, emulsification quality is evaluated by several parameters defined as follows.

The arithmetic mean diameter of the droplets D_{10}:

$$D_{10} = \frac{1}{n}\sum_1^n D_i \tag{1}$$

Where n is the number of the analyzed droplets, D_i denotes the diameter of each droplet.

Based on the arithmetic mean diameter, the standard deviation is calculated as:

$$\delta = \sqrt{\frac{\sum_1^n (D_i - D_{10})^2}{n}} \tag{2}$$

The Sauter mean diameter (SMD), D_{32}, is defined as the diameter of a sphere that has the same volume/surface area ratio as a collection of droplets. This parameter is important since the active surface between oil-water two phases in the emulsion implies the potential interfacial energy stored. The calculation is given as:

$$D_{32} = \frac{\sum_1^n {D_i}^3}{\sum_1^n {D_i}^2} \tag{3}$$

Another essential parameter is the polydispersity index (*PdI*), which is the indicator of the size distribution uniformity. A low value of *PdI* implies that droplets are rather monodispersed. The ideal monodispersed emulsion has *PdI* value equaling to zero. Polydispersity index is defined as the square of the standard deviation-to-arithmetic mean diameter ratio:

$$PdI = \left(\frac{\delta}{D_{10}}\right)^2 \tag{4}$$

Fig.5 shows the evolution of the arithmetic mean diameter of the droplets (D_{10}) versus the considered number of droplets in an emulsion obtained from the asymmetric configuration for one flow rate example case. It is confirmed that the mean drop diameter gets convergent via this automated granulometry procedure. Also, it has been verified that the final results of D_{10} from automated granulometry and these from manual analysis agree well, which validates the fidelity of the automated granulometry method.

2.4 Flow visualization

The flow visualization is carried out to observe the interaction of oil and water streams by a Photron fast speed camera (FASTCAME SA-X2 1080K M4), whose maximum frame rate is 1080 kHz. To balance the spatial and temporal resolutions, the shooting frame rate in the present study on flow patterns is selected to be 300 kHz, hence the exposure time is limited to be the longest available (1/583784 in seconds) for this frequency. A Lavision high magnification (12×) zoom lens is used to allow observations at the micrometer scale in the emulsification facility. The focus of the lens is adjusted in the channel depth. Considering the region of interest in the observation, the spatial resolution is 4 μm /pixel. Because of high speed capturing images with such a large zoom lens at so short exposure time, an external powerful light source is necessary to illuminate the microchannel crossroad. This one should generate a signal strong enough to be recorded by the camera. Therefore, a 50 W Halogen lamp is located on the opposite side and facing the camera beyond the transparent microchannel to enhance the brightness to a great extent. Attention is paid to the fact that the use of the lamp does not warm up the fluid flowing through the studied microsystem.

2.5 Test conditions

As mentioned above, the continuous and dispersed phases used for o/w emulsification are water and rapeseed oil, respectively. Their main characteristics at 25°C are recapped in Tab.1. The surface tension and interfacial tension have been measured using a Kruss K-12 tensiometer using the Wilhelmy method. The viscosity of the fluids has been obtained using a Thermo Scientific Haake Mars III rheometer. The uncertainty of the tension and viscosity measurements are estimated to be respectively 5% and 1%.

Tab.1. Characteristics of the used fluids (at 25°C).

Liquids at 25°C	Tap water	Rapeseed oil
ρ (kg/m^3)	998	865
μ (mPa s)	0.91	52.2
γ (mN/m)	73.5	33.7
σ (mN/m)	27.6(without surfactant)/ 7.4 (with 0.5% Tween as surfactant)	

To compare the two configurations at different flow conditions, flowrates of water and oil are pre-set and input into the pump control systems based on targeted Reynolds number and oil volume fraction in the emulsion, as summarized in Tab.2. Reynolds number based on the aqueous phase is designed to be in so-called "low", "medium" and "high" levels by modulating water flowrate as 50 mL/min, 100 mL/min, and 150 mL/min. Accordingly, Reynolds number based on the continuous phase properties and water inlet channel dimension (Re_c) are 1524, 3047, and 4570. And oil to water volume ratio ($f = \dot{V}_d/\dot{V}_c$) in the emulsion is set from 10% to 25% with an interval of 5%. Moreover, to allow correct microscopy imaging, 0.5% TWEEN 20 is dissolved in the water to stabilize the emulsion sample for microscopy imaging. Tween 20 is polyoxyethylene sorbitol ester. It is an anionic tensioactive molecule which belongs to the polysorbate family and that is largely used for stabilizing oil in water emulsions. Its molecular weight is about 1225 Daltons.

Tab.2. Test matrix for studying asymmetric configuration and symmetric one.

$\dot{V}_c$ (mL/min)	$\dot{V}_d$ (mL/min)	Re_c	f
50	5, 7.5, 10, 12.5	1524	10%, 15%, 20%, 25%
100	10, 15, 20, 25	3047	
150	15, 22.5, 30, 37.5	4570	

Measurement trails on droplet size and size distribution without Tween 20 has been done to elucidate the effect the surfactant. However, it is inappropriate to do this by current non-in-situ microscopic method because the droplets will coalescence quickly during the sample collection, preparation of the microscopic slice and images recording, especially in our studied case where the oil phase can be fragmented into very small drops initially. On the trial of microscopic observation of emulsion sample without surfactant added, the merging process of several small drops into a large one is even witnessed.

3. Results and discussion

3.1 Drop size distribution

With abundant drops size measurements allowed by automated granulometry, statistical analysis is thus carried out to check its distribution for both configurations. Fig.6 plots the comparison of cumulative distribution function (*c.d.f*) at the smaller flow rate conditions with varied dispersed oil fraction. It can be noticed from Fig.6(a) that the cumulative probability ramps up rapidly at the range where drops are small, i.e. 1 to 10 μm. For instance, drops with a diameter less than 10 μm occupy as high as 80% in the final populations. Within this range of droplet size, no significant difference between two cross-slot geometries can be distinguished. The ability and efficiency of the studied two-stream impinging microfluidics working at high throughput in terms of producing fine dispersed drops is proven. Disparities between the two configurations show up in the range of relatively bigger drops size as marked with the green box in Fig.6(a) and zoomed-in details are presented in Fig.6(b). In general, the flow pattern inside asymmetric cross-slot configuration induces the formation of more large drops than with the fully symmetric one, so the cumulative probability distribution curves for the symmetric configuration converge to 100% faster at all tested oil fraction cases. As for the effect of the dispersed phase volume ratio in the emulsion, increasing oil fraction in such emulsifiers leads to higher oil flowrates transported into the collision region. Thus, more momentum is carried, leading to more intense interactions with the head-on water flow. As a result, oil streams are dispersed as finer droplets at higher oil fraction cases.

Not demonstrated by the cumulative probability, variations of the drop size distribution for the two configurations in the small-drop size range [0-20μm] is plotted in Fig.7 at Re_c of 1524, with the oil fraction of 10%. The probability distribution agrees well with the lognormal distribution; this is consistent with the fact that the dispersed phase undergoes statistically mostly several successive events of break-up (Ji et al. 2021). It indicates that the symmetric configuration shows strength in generating finer dispersions than the asymmetric one. To be specific, concerning the peaks of the droplets granulometries, a frequency of droplets in the range [2-3 μm] of (30%) is obtained in the symmetric cross-slot microchannel, while a frequency of 25% is observed for a relatively larger diameter range [3-4 μm] in the asymmetric device. Besides, the drop size distribution of the asymmetric configuration spreads in a wider diameter range, meaning that the created emulsion is more polydisperse.

Both *c.d.f* and *p.d.f* results show that the studied microchannel with the symmetric cross-slot geometric layout is more efficient to disperse the oil phase into the water as relatively smaller droplets than the asymmetric one at studied low *Re* conditions. This can also be directly observed by the microscopy images taken at one example case, as shown in Fig.8. The maximum diameter (D_{max}) measured respectively in the symmetric and asymmetric configurations at this condition (Re_c =1524 and f =10%) in the symmetric and asymmetric configurations are 117 μm and 135 μm, as shown in Tab.3. The reason could be that shear stress involved in the symmetric configuration is higher than that in the asymmetric one. This may be explained by the rearrangement of the velocity profile in the impingement region, allowing the disruptive force exerted on the dispersed oil phase to be greater, which will be disclosed in the following discussion on flow visualizations. However, the single macro swirl previously observed (Belkadi et al. 2016) in the asymmetric one changes to a counter-rotating swirl pair in the symmetric configuration, which is expected to enhance the mixing of the two-phase flow better. On the other hand, it has to be pointed out that the disparities between the two geometries are not so great. The final

o/w emulsion quality is not only determined by the configurations of the crossroad where the two inlet streams impact, the downstream elbows also helps to breakdown the instability generated inside the microchannel and refine the emulsion further.

As the flowrate is elevated, not only the velocity gradient, which determines the disruptive shear stress but also the kinetic energy induced into the collision region to mix the two-phase flows gets higher. Consequently, the oil droplets size is reduced, as presented in Fig.9, which shows the cumulative probability distribution at medium Re studied condition (Re_c=3047). Again, taking the reference *c.d.f* value (80%) to compare with the low Re conditions (Re_c=1524), more than 80% of drops are smaller than 7 μm at Re_c=3047 for all oil fraction cases (see Tab.3). Regarding the configuration comparison, the cumulative probability curves keep almost same for two cross-slot layouts under different oil fraction conditions in the range of smaller drop size regime [0-4 μm]. As pointed out with the box framed in green in Fig.9(a) and magnified in Fig.9(b), a slight difference of the *c.d.f* curves can also be noticed in the range of larger droplets size, like what has been illustrated at the low Re condition, the symmetric configuration tends to generate more small drops than the asymmetric one resulting in the *c.d.f* climbing up to reach 100% a little more rapidly. The maximum diameters for the asymmetric and symmetric geometries are 112 μm and 105 μm, respectively (see Tab.3). The effect of the oil fraction is also similar to the low Re case.

As stated, symmetric configuration exhibits a certain superiority in promoting the dispersion process thus causing finer oil droplets distributed in the final emulsion. But as the flow rates of both phases increase further, the geometry of the cross-lot seems to have less and less influence on the drop size distribution. Fig.10 shows cumulative probability evolution at the highest Re condition investigated in the present study (Re_c=4570). Surely, two phases with higher momentum impinging with each other at the compact microchannel allow getting smaller droplet size generally. The maximum diameter detected at this high Re condition is below 70 μm (shown in Tab.3). The drop size distributions obtained after emulsification with varying oil fraction rate are also very close, the cumulative probability curves being quite coincident.

More in detail, Fig.11 presents the drop diameter probability distribution for two configurations in the small-drop range [0-20 μm] at Re_c of 4570 with the oil fraction of 10%. The log-normal distribution function is fitted well for both configurations. There is little difference between the two configurations since fitting curves are nearly consistent. If compared with Fig.7, it is observed that the peak probability is over 35% for the diameter range [2-3 μm] for both configurations, while this peak value is below 30%, especially for the asymmetric configuration at low Re condition.

A significant decline of the drop size can also be seen from microscopy images directly in Fig.12. At the same oil fraction condition, oil droplets are more densely and uniformly at the high Re condition. Similarly, the emulsification performance of the symmetric and asymmetric geometries layouts is close to each other in terms of similar dispersed distribution performance.

Drop size distributions give detailed information of o/w emulsion quality fabricated by studied head-on impingement microfluidic device, which is useful to compare the asymmetric and symmetric configurations of the cross-slot layout. In general, it can be concluded that the symmetric configuration works better than the asymmetric one because of generating finer oil droplets, especially at low Re tested conditions. Except for the drop size distribution, averaged outcomes will also be discussed in the following to further disclose the hydrodynamic and geometric effects on the global emulsion quality in the microchannel.

3.2 Mean drop size & emulsification efficiency

Fig.13 depicts the arithmetic mean drop diameter (D_{10}) for tested conditions. Overall, the particular designed microfluidic microsystem tested in this study at the conditions of great amounts of dissipated kinetic energy leads to averaged drop diameters less than 10 μm at all experimental cases. The efficiency of the microchannel utilizing continuous and dispersed phase streams to impinge with each other is exhibited here. No matter how the cross-slot is arranged geometrically, the averaged drop diameter decreases with Re. At a given dispersed volume fraction, higher flowrate continuous phase flow induces higher disruptive stress acted on the oil streams for fragmentation, thus making it highly finely dispersed in the water environment. This phenomenon has already been described by previous studies implemented with several microfluidic configurations, using different flow range conditions and for oil in water or water in oil emulsions. Tan et al. (2006), for example, have pointed out that the decreasing of the droplet radius follows a simple power-law function where the flow rate of the continuous phase (oil) is at the power of -0.27 to -0.34, depending on the fixed dispersed phase (water)

flowrate. These experiments concerned very tiny values of the flowrates ($\sim\mu L/min$) and the smallest value of the drop diameter measured was about 30 μm. The trends indicate that drop size can't unlimitedly be reduced for a given geometry and flow conditions. Under the present conditions, it is not possible to break the oil droplets less than 1 μm. It is also confirmed that the gap between the medium and high Re conditions is less than that between the low and medium Re conditions. The minimum averaged drop diameter measured is presently 3.9 μm. In the same order of ideas, at a given water flow rate, D_{10} reduces as the oil flowrate increases if the water flow rate is kept because of the higher oil flow momentum imposed. However, it seems to converge to a critical value, which is reasonable because emulsion conversion from o/w to w/o emulsion will take place if more and more oil is input. Fig.13 indicates the better performance of the symmetric configuration, especially at low Re conditions. It then can be summarized that cross-slot geometry shows greater influence at the small flow conditions. As Re increases, the averaged drop diameter is mainly dependent on the hydrodynamic situation inside the microchannel, so the impact of the impingement configuration weakens. To be specific, the mean drop diameter in the symmetric head-on collision microchannel is averagely 11% smaller compared with the asymmetric configuration at low Re conditions (Re_c=1524). At high Re conditions (Re_c=4570), this scatter is reduced to 7%.

The Sauter mean diameter presents the same trend as the arithmetic mean diameter, as plotted in Fig.14. It also declines as Re or f is promoted. And the difference between the two configurations is consistent with that characterized by arithmetic diameter. D_{32} is shown to be much larger than D_{10} because the oil-in-water emulsion fabricated by the studied microsystem is polydisperse. The correlation between the Sauter mean diameter and the arithmetic mean diameter for symmetric and asymmetric configurations are shown in the following formula (5) and (6) respectively:

Symmetric configuration: $$D_{32} = 6.15 * D_{10} - 15.7 \quad (5)$$

Asymmetric configuration: $$D_{32} = 5.06 * D_{10} - 10.1 \quad (6)$$

Our microchannel is designed to work at high throughput, thus the emulsion produced is not a typical mono-dispersed system like with conventional droplet-based microfluidics. Polydispersity defined in Eq.(4), is presented in Fig.15. This figure indicates that enhancing the value of the Reynolds number or the oil fraction allows narrowing the size scattering range of the oil fragments. For example, at the lowest Re_c condition ($Re_c = 1524$), the polydispersity is as high as 2.54 when the oil fraction is only 10% for the asymmetric configuration, and it decreases to 1.65 (by 35%) at the highest f case (f=25%). When the flow rate grows to the maximum case investigated ($Re_c = 4570$), PdI drops a lot, from 1.13 to 0.84. It can also be noticed that polydispersity varies less with adjusting dispersed oil phase fractions at higher Re. Impinging the continuous and dispersed phase co-axially is beneficial to make the final emulsions less heterogeneous. This advantage of the symmetric configuration is not that significant when the flowrate is promoted to the highest. Specifically, at the highest oil fraction condition (f=25%), PdI for the symmetric configuration is 1.16 when Re_c is low ($Re_c = 1524$), and it is 1.75 for the asymmetric configuration, which enhances 51%. But this enhancement declines to 12% as Re_c is elevated to 4570 ($PdI = 0.75$ for the symmetric configuration and 0.84 for the asymmetric one).

Discussion on the averaged drop diameter confirms the conclusion reached from the drop size distribution. The symmetric configuration generally is superior to the asymmetric one in terms of smaller oil droplets created in the emulsions. From the perspective of uniformity of the distributed oil droplets, the symmetric configuration also performs better. But the advantage vanishes as the working flow rate is increased.

For scaling the droplet size with the hydrodynamic conditions including both continuous and dispersed phase, it is found that the arithmetic mean drop diameter is in a power law correlation with Weber number defined as the following:

$$We = \frac{\rho_d U_e^2 D_{h_d}}{\sigma} \quad (7)$$

Where ρ_d is the density of the dispersed phase. U_e is the velocity of the emulsion in one outlet channel, which is driven by both water and oil flowrates and D_{h_d} is the hydrodynamic diameter of the oil channel. Data and their fitting curves are superimposed in Fig.16. The arithmetic mean diameter is in a relation of $We^{-0.25}$ for the symmetric configuration, and it is $We^{-0.27}$ for the asymmetric configuration. Also, the red dot line is the result for integrating results of both configurations, showing the power index of the scaling law is between that for two configurations separately. Assuming the power index is roughly -0.25 for both configurations, it means that $D_{10} \propto \frac{1}{We^{0.25}} \propto \frac{1}{U_e^{0.5}}$. So D_{10} is in a linear correlation with $\frac{1}{\sqrt{U_e}}$. It indicates that the averaged drop size of o/w

emulsions generated by the investigated microfluidic device is dominated by the flow velocity of the emulsion flow.

It is not enough to determine whether an emulsifier is good or not only by evaluating the outcome emulsion quality only, the cost of dissipated energy per mass of emulsion is also a paramount parameter. To this end, the energy consumption per mass of emulsion is estimated as:

$$E = \frac{\dot{m}_c \frac{\Delta P_c}{\rho_c} + \dot{m}_d \frac{\Delta P_d}{\rho_d}}{\dot{m}_c + \dot{m}_d} \tag{8}$$

Where, ΔP_c and ΔP_d are the pressure drops for the continuous and dispersed phase, respectively. The dissipated energy is compared to the created liquid-liquid interface surface area per volume of emulsion, i.e. a specific surface area (S_p).

$$S_p = 6\varphi_d / D_{32} \tag{9}$$

Where φ_d is the oil volume fraction in the emulsion [$\varphi_d = \dot{V}_d/(V_c + \dot{V}_d)$].

Fig.17 presents the created specific surface area, S_p, as a function of the energy dissipated by per unit mass of emulsion. It can be observed that the created interface per volume of emulsion increase roughly linearly with the energy expended. The asymmetric configuration appears to be more efficient considering this criterion. Although the symmetric configuration assists to manufacture smaller and more uniform oil droplets than the asymmetric configuration, it requires relatively more energy to fulfill this. Fig.18 also illustrates this point by unrevealing the correlation of mean drop diameter to energy dissipation in different systems. From this point of view, the asymmetric cross-slot geometry is slightly more energy-saving.

It has to be noted that the asymmetric device has been originally designed for fabricating W/O emulsion (water emulsified in biodiesel) as it was developed for energy application (Marchitto et al. 2018; Belkadi et al. 2016), which can be realized by simply switching the inlet phases in practice. Since the device works at high throughput, the effect of the surface energy is negligible. Therefore, PMMA and aluminum systems, for example, provide same quality of emulsions. It can be viewed as another advantage of the current microsystem.

3.3 Flow visualization

Optical visualization of flow in the vicinity of the impingement region is carried out using high-speed camera photography. Fig.19 displays the oil and water flow interactions at the low *Re* condition for both configurations with the oil fraction varying from 10% to 25%. The oil/water interface appears in black. The observation window is diagramed on the top of Fig.19. When the oil fraction is the lowest, Fig.19(a), the macro swirl flow triggered in the asymmetric configuration rolls up the oil stream after impacting with the oncoming water stream in the crossroad: the interface firstly takes the form of a tile, the concave part of which is located in the direction of the water inlet. The oil phase is then twisted and flows towards the outlet as a stable filament having a thickness of about 200 μm. This means that the break-up of the oil phase mainly occurs downward, at this flowrate. In these conditions, the oil filament is located on the side of the oil inlet. On the opposite, in the symmetric configuration at the same flow condition (Fig.19(e)), the water stream rolls the oil stream more intensely and the interface longer keeps the shape of a large tile. Developing to the downstream, the instability shows up at the two ends of the observation window, which is caused by the higher shear stress between two-phase liquids.

With the increment of oil fraction, instability is also generated in the asymmetric configuration (Fig.19(b)), resulting in the creation of unstable long strips of the interface, as marked in the red dashed circles. Thanks to the improvement of shear stress, oil streams tend to split into many long and thin filaments in the symmetric configuration at comparable conditions, as shown in Fig.19(f). What can be expected is that these thin filaments will be disrupted into droplets further downstream. The interaction between two-phase liquids is more intensified when the flow rate of oil is further promoted to 15%, making the oil-water impacting interface more corrugated for the asymmetric configuration (Fig.19(c)) and much thinner filaments shedding off from the oil streams (Fig.19(g)). Finally, the enhancement of the shear-stress induced instability is not that evident in the asymmetric configuration (Fig.19(d)). Only some local instability is captured near the edge of the water channel exit, as shown in Fig.20 in detail. The corrugated thin filament is cut off (t=0.137 ms). The instability continues to develop on the residue portion (marked with the red circle) and propagates to the downstream with a great extension (t=0.683 ms), which disappears at last (t=1.230 ms). What is interesting is that fine helical filaments (Fig.19(h)) are observed in the symmetric configuration, which is attributed to the effect of the dual swirl motion. Moreover, oil flows with higher momentum push the oil-water initial interface away from the side of the oil inlet.

The most dominant external force imposed on the dispersed phase at low Re conditions is the shear stress, which is dependent on the velocity gradient across the interface. However, it will switch to turbulent pressure fluctuations of the flow inside the microchannel as the Re increases a lot. So the interaction between the two-phase flows looks more chaotic, especially at high Re conditions, as displayed in Fig.21. In the medium Re regime, both shear stress and turbulent fluctuation could be possibly responsible for the dispersed phase breakage, therefore visible large drops begin to appear along with filaments (Fig.21(a)&(d)). At the highest Re investigated here, a great amount of small drops is formed from the oil phase fragmentation (Fig.21(b)&(e)); finer structures are observed in the symmetrical geometry. Oil streams in the outlet are rapidly burst into clouds of small drops at the elevated oil fraction (Fig.21(c)&(f)). The difference is difficult to be distinguished between two configurations in this most intensified case, even if the area involved by the formation of interfaces seems to be a bit larger in the symmetric geometry, which is globally consistent with the conclusions reached in the drop size and size distribution part.

The modulation of the velocity profile in the impingement region by arranging different cross-slot layouts enhances the velocity gradient thus the shear stress for the symmetric configurations, which results in the finer and more uniform oil droplets distributed in the created emulsions in the low Re regime. With the increase of the flow rate of oil and water phases, the instability inside the flow augments greatly and even fully turbulent emulsification can be reached. At this status, the disparity between two configurations in terms of drop size is diminished since the interaction intensity is high enough. On the other hand, the intrinsic property of higher instability in the symmetric configuration causes the higher energy cost at the same flow conditions.

4. Conclusions

In the present study, experimental work is carried out to characterize the oil-in-water emulsification performance in the head-on impingement microchannels designed to work at high throughput. Effect of the layout of the water and oil inlet channels in the cross-slot is examined by measuring the drop size and size distributions at varied continuous and dispersed phase flowrates via microscopy analysis associated with automated granulometry. Depending on the relative positions of the two inlet channels axes, the symmetric and asymmetric configurations are denoted. Emulsification efficiency in terms of the energy cost for per created emulsions is compared. Flow visualization is also performed to get the insight of the two-phase flow interactions in the studied microfluidic devices.

The microsystems utilize the kinetic energy carried by two face-to-face streams for o/w emulsification through collision in the extremely compact confinement, which helps to fabricate very fine oil droplets distributed in the created emulsion. The arithmetic mean diameter is less than 10 μm at all experimental cases, and the minimum mean drop diameter, 3.9 μm, is obtained at the highest energy dissipation condition. The difference of droplet size distribution between the two configurations is not distinguished in the small drop diameter range but tends to show up in the relatively larger drop size range. Generally, the symmetric cross-slot geometry works better than the asymmetric one allowing to produce a smaller number of large droplets and dispersing the oil phase more uniformly at the same hydrodynamic conditions, especially when Re is low. As flowrates of both phase increases, the disparity is diminished. The arithmetic mean drop diameter in both systems is found to be scaled with the Weber number, which is defined based on the velocity of the emulsion. The symmetric configuration shows an advantage in manufacturing finer and less poly-dispersed emulsions than the asymmetric one at given flow conditions. However, it demands relatively higher energy cost and its manufacturing is less simple.

The mechanism of the strength showed by the symmetric configuration in generating better quality o/w emulsions is discovered by observing the oil and water flow interactions when they collide. It is concluded that the velocity profile in the impingement region is significantly modulated by arranging different cross-slot layouts. Thus, velocity gradient induced shear stress in the symmetric configurations is greater than in the asymmetric one, which leads to smaller and more uniform oil droplets disrupted in the two liquids dispersion system in the low Re flow regime. Instability in the symmetric configuration also exceeds the other one, which brings in more intensified interaction and mixing. The gap between two configurations in terms of drop size is narrowed when the interaction is intense enough with the increment of the flowrates. The intrinsic higher instability feature in the symmetric configuration is responsible for the higher energy cost at the same working flow conditions as the asymmetric configuration. Considering the choice of an adequate configuration, the balance has to be considered between flowrates involved, needed quality, and cost of dissipated energy as well as device manufacturing.

Declarations

Funding: Région Pays de la Loire (Chaire "Connect Talent") on Optical Diagnostics for Energy.
Conflicts of interest: Not applicable
Availability of data and material: Not applicable
Code availability: Not applicable
Author Contributions: Yongbin Ji: Formal analysis and investigation, Writing original draft; **Jérôme Bellettre:** Conceptualization, Project administration, Funding acquisition, Supervision; **Agnès Montillet:** Conceptualization, Formal analysis, Validation; **Patrizio Massoli:** Methodology, Funding acquisition, Supervision.

Appendix: Summarized experimental results.

Tab.3. Drop size measurement data for all tested cases.

	System	$\dot{V}_w$ (mL/min)	$\dot{V}_o$ (mL/min)	D_{10} (μm)	D_{32} (μm)	PdI	D_{max} (μm)	$D_{80\%}$ * (μm)
Low Re (Re_c=1524)	Symmetric Conf.	50.8	5.0	8.0	36.0	2.34	117.0	8.3
		49.9	8.1	6.8	26.5	1.59	111.2	8.0
		46.6	10.9	6.5	21.3	1.49	108.4	7.8
		48.4	12.7	6.2	17.7	1.16	106.9	7.5
	Asymmetric Conf.	49.7	4.6	8.6	37.4	2.54	135.2	9.3
		49.5	7.1	8.2	34.0	2.23	124.9	9.1
		50.4	9.7	7.6	22.1	1.75	118.4	8.5
		49.7	11.9	6.8	22.0	1.65	116.5	7.6
Medium Re (Re_c=3047)	Symmetric Conf.	94.8	9.9	4.8	20.0	1.41	104.7	5.3
		102.4	15.0	4.7	13.9	1.14	96.3	5.2
		103.8	20.1	4.7	10.3	0.78	88.1	5.1
		103.2	23.4	4.6	10.6	0.74	80.9	5.1
	Asymmetric Conf.	96.7	10.4	5.5	22.4	1.57	112.4	6.3
		96.7	15.7	5.4	19.4	1.44	97.9	5.9
		96.7	20.9	5.4	15.1	1.25	92.9	5.6
		98.1	25.9	4.8	13.9	1.09	90.2	5.4
High Re (Re_c=4570)	Symmetric Conf.	158.0	15.6	4.3	10.6	0.89	59.2	4.9
		157.1	22.7	4.0	11.1	0.81	49.1	4.4
		151.8	30.9	4.0	8.1	0.68	48.8	4.2
		152.1	37.1	3.9	8.8	0.75	46.7	4.2
	Asymmetric Conf.	150.8	16.5	4.6	14.6	1.13	78.4	5.0
		151.0	25.1	4.5	13.6	0.97	66.3	4.8
		149.9	30.7	4.3	9.6	0.74	66.2	4.8
		149.1	38.3	4.1	10.3	0.84	63.8	4.8

* $D_{80\%}$ is the critical diameter of *c.d.f* reaching 80%.

References

Abismail B, Canselier JP, Wilhelm AM, Delmas, H, Gourdon C (1999) Emulsification by ultrasound: drop size distribution and stability. Ultrason Sonochemistry 6:75-83.

Ait Mouheb N, Montillet A, Solliec C, Havlica J, Legentilhomme P, Comiti J, Tihon J (2011) Flow characterization in T-shaped and cross-shaped micromixers. Microfluid Nanofluid 20:1185-1197.

Anna SL, Bontoux N, Stone HA (2003) Formation of dispersions using "flow focusing" in microchannels. Appl Phys Lett 82:364-366.

Belkadi A, Montillet A, Bellettre J, (2018) Biofuel emulsifier using high-velocity impinging flows and singularities in microchannels. J Energ Resour Technol 140:012202.

Belkadi A, Tarlet D, Montillet A, Bellettre J, Massoli P (2016) Study of two impinging flow microsystems arranged in series. Application to emulsified biofuel production. Fuel 170:185-196.

Bellettre J, Belkadi A, Montillet A (2017) https://bases-brevets.inpi.fr/fr/document/WO2017103498.html

Bothe D, Stemich D, Warnecke HJ(2006) Fluid mixing in a T-shaped micro-mixer. Chem Eng Sci 61:2950-2958.

Chen HT, Middleman S (1967) Drop size distribution in agitated liquid-liquid systems. AIChE J 13:989-995.

Cohen C, Giles R, Sergeyeva V, Mittal N, Tabeling P, Zerrouki D, Baudry J, Bibette J, Bremond N (2014) Parallelised production of fine and calibrated emulsions by coupling flow-focusing technique and partial wetting phenomenon. Microfluid Nanofluid 17:959-966.

Cramer C, Fischer P, Windhab EJ (2004) Drop formation in a co-flowing ambient fluid. Chem Eng Sci 59:3045-3058.

Davies JT (1985) Drop sizes of emulsions related to turbulent energy dissipation rates. Chem Eng Sci 40:839-842.

Galus S, Kadzińska J (2015) Food applications of emulsion-based edible films and coatings. Trends Food Sci Technol 45:273-283.

Habchi C, Lemenand T, Valle DD, Peerhossani H (2009) Liquid/liquid dispersion in a chaotic advection flow. Int J Multiphase Flow 35:485-497.

Ji Y, Bellettre J, Montillet A, Massoli P (2020) Fast oil-in-water emulsification in microchannel using head-on impinging configuration: Effect of swirl motion. Int J Multiphase Flow 131:103402.

Ji Y, Bellettre J, Montillet A, Massoli P (2021) Experimental investigation on single drop breakage in two-stream impinging microchannels. Exp Fluids 62:17.

Kiljański T (2004) Preparation of emulsions using imping streams. AIChE J. 50:1636–1639.

Kilpatrick PK (2012) Water-in-crude oil emulsion stabilization: Review and unanswered questions. Energy Fuels 26:4017-4026.

Kobayashi I, Takano T, Meada R, Wada Y, Uemura K, Nakajima M (2008) Straight-through microchannel devices for generating monodisperse emulsion droplets several microns in size. Microfluid Nanofluid 4:167-177.

Kolmogorov AN (1949) On the breakage of drops in a turbulent flow. Dokl Akad Nauk S S S R 66:825-828.

Lawrence MJ, Rees GD (2000). Microemulsion-based media as novel drug delivery systems. Adv Drug Deliv Rev 45:89-121.

Lemenand T, Della Valle D, Zellouf Y, Peerhossaini H (2003) Droplets formation in turbulent mixing of two immiscible fluids in a new type of static mixer. Int J Multiphase Flow 29:813-840.

Lemenand T, Habchi C, Della Valle D, Bellettre J, Peerhossaini H (2014) Mass Transfer and emulsification by chaotic advection. Int J Heat Mass Transf 71:228-235.

Luo J, Chu G, Luo Y, Zou H, Li G, Chen J (2017) Experimental investigations of liquid-liquid dispersion in a novel helical tube reactor. Chem Eng Process 117:162-170.

Mahajan AJ, Kirwan D J (1996) Micromixing effects in a two-impinging-jets precipitator. AIChE J 42:1802-1814.

Marchitto L, Calabria R, Tornatore C, Bellettre J, Massoli P, Montillet A, Valentino G (2018) Optical investigations in a CI engine fueled with water in diesel emulsion produced through microchannels. Exp Therm Fluid Sci 95:96-103.

Moreira A, Carneiro J, Campos JBLM, Miranda JM (2021) Production of hydrogel microparticles in microfluidic devices : a review. Microfluid Nanofluid 25:10.

Nakashima T, Shimizu M (1988) Advanced inorganic separative membranes and their new developments. Chem Eng Symp Ser 21:93.

Paquin P (1999) Technological properties of high pressure homogenizers: the effect of fat globules, milk proteins, and polysaccharides. Int Dairy J 9:329-335.

Perro A, Nicolet C, Angly J, Lecomandoux S, le Meins JF, Colin A (2011) Mastering a double emulsion in a simple co-flow microfluidic to generate complex polymersomes. Langmuir 27:9034-9042.

Rayleigh L (1878) On the instability of jets. Proc Lond Math Soc 10:4–13.

Schlender M, Spengler A, Schuchmann HP (2015) High pressure emulsion formation in cylindrical coaxial orifices: Influence of cavitation induced pattern on oil drop size. Int J Multiphase Flow 74:84-95.

Siddiqui SW (2014) The effects of oils, low molecular weight emulsifiers and hydrodynamics on oil-in-water emulsification in confined impinging jet mixer. Colloids Surf A Physicochemical Eng Asp 443:8-18.

Siddiqui SW, Norton IT (2012) Oil-in-water emulsification using confined impinging jets. J Colloid Interface Sci 337:213-221.

Solsvik J, Jakobsen HA (2015) Single drop breakup experiments in stirred liquid-liquid tank. Chem Eng Sci 131:219-234.

Taha A, Ahmed E, Ismaiel A, Ashokkumar M, Xu X, Pan S, Hu H (2020) Ultrasonic emulsification: An overview on the preparation of different emulsifiers-stabilized emulsions. Trends Food Sci Technol 105:363-377.

Tamir A, Sobhi S (1985) A new two-impinging-streams emulsifier. AIChE J 31:2089-2092.

Tan YC, Cristini V, Lee AP (2006) Monodispersed microfluidic droplet generation by shear focusing microfluidic device. Sen Actuators B Chem 114:350-356.
Taylor GI (1932) The viscosity of a fluid containing small drops of another fluid. Proc Roy Soc 138:41-48.
Theron F, Sauze NL (2011) Comparison between three static mixers for emulsification in turbulent flow. Int J Multiphase Flow 37:488-500.
Thorsen T, Roberts RW, Arnold FH, Quake SR (2001) Dynamic pattern formation in a vesicle-generating microfluidic device. Phys Rev Lett 86:4163-4166.
Tsaoulidis D, Angeli P (2017) Liquid-liquid dispersions in intensified impinging-jets cells. Chem Eng Sci 171: 149-159.
Ushikubo FY, Birribilli FS, Oliveira DRB, Cunha RL (2014) Y- AND T-junction microfluidic devices: effect of fluids and interface properties and operating conditions. Microfluid Nanofluid 17:711-720.
Vladisavljević GT, Kobayashi I, Nakajima M (2012) Production of uniform droplets using membrane, microchannel and microfluidic emulsification devices. Microfluid Nanofluid 13:151-178.
You JB, Choi Y, Im SG (2017) Influence of adjusting the inlet channel confluence angle on mixing behavior in inertial microfluidic mixers. Microfluid Nanofluid 21:121.
Zhao CX, Middelberg APJ (2011) Two-phase microfluidic flows. Chem Eng Sci 66:1394-1411.
Zhu P, Wang L (2017) Passive and active droplet generation with microfluidics: a review. Lab Chip 17:34-75.

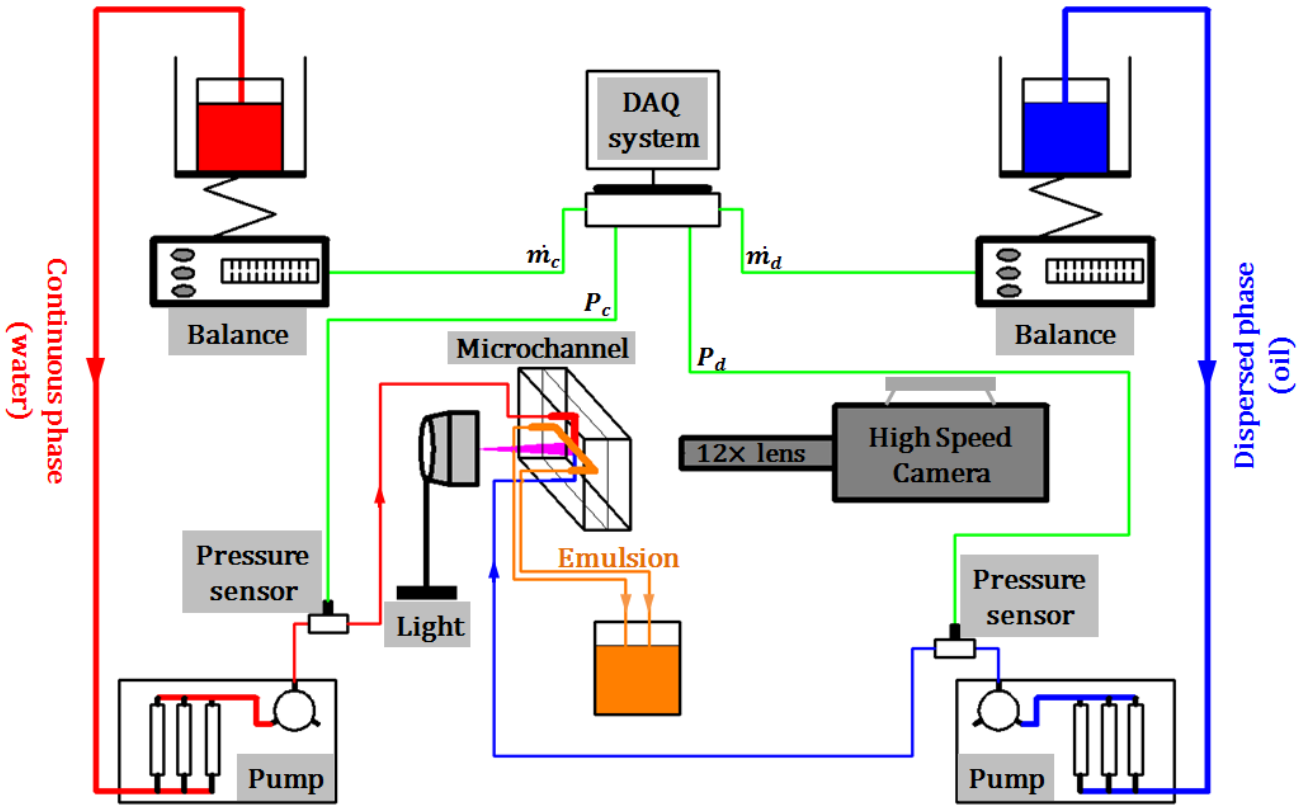

Fig. 1. Experimental setup for oil-in-water emulsification.

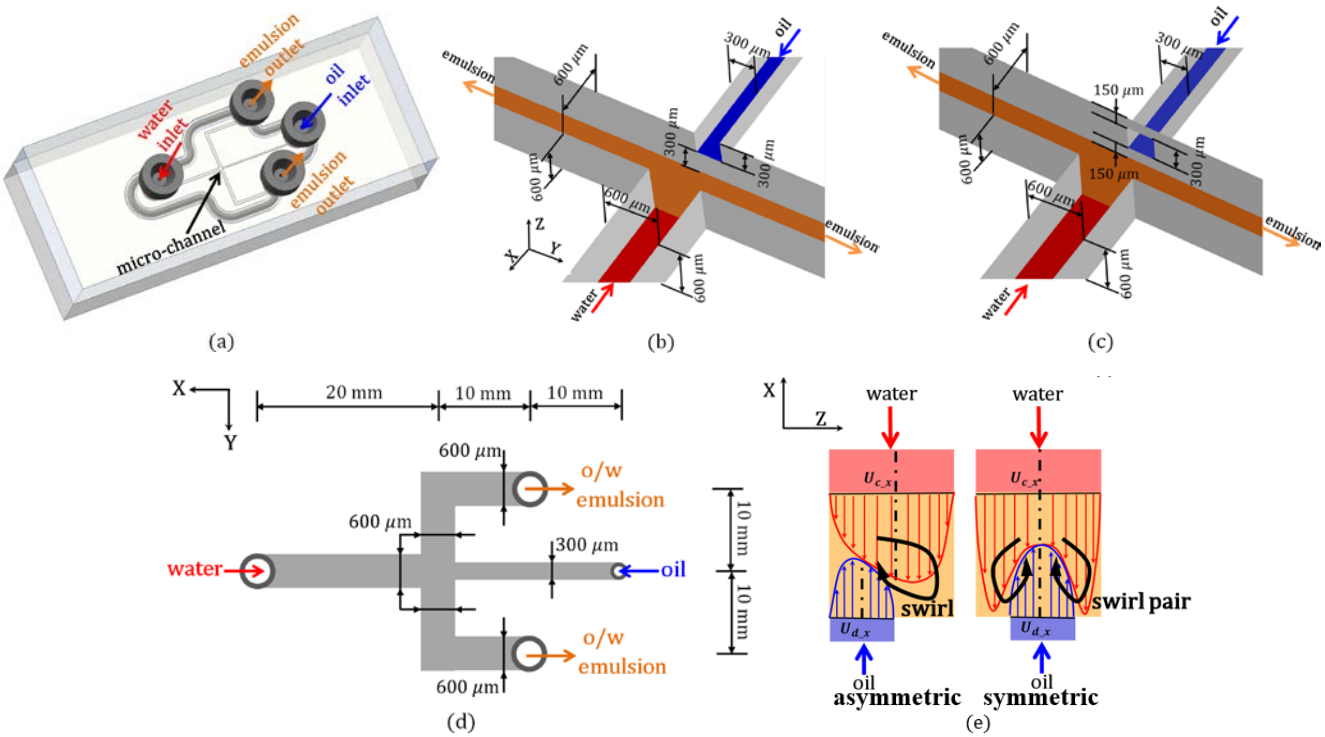

Fig. 2. The microchannel system: (a)microfluidic emulsification device; (b)asymmetric cross-slot configuration; (c)symmetric cross-slot configuration; (d)XY plane; (e)XZ plane.

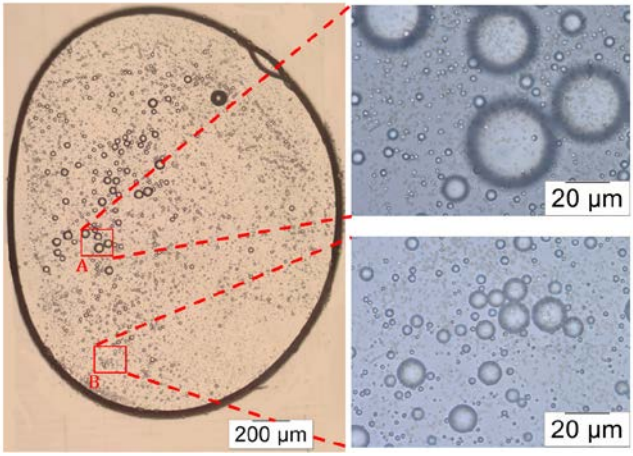

Fig.3. Typical microscope image at 5× and 50× magnification.

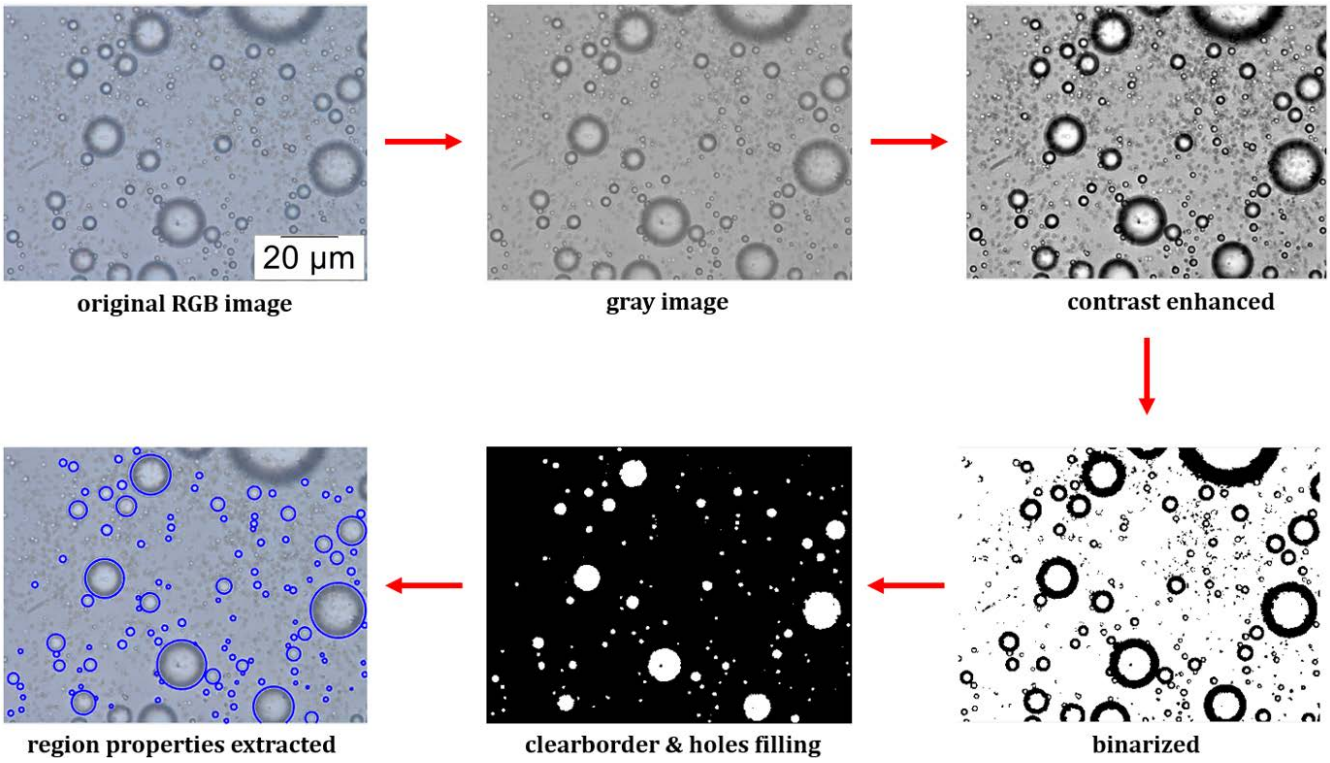

Fig.4. Microscopy images processing procedure.

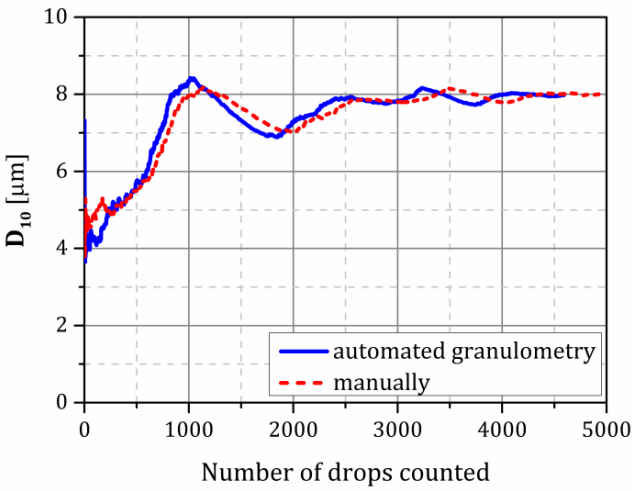

Fig.5. Convergence of mean droplet diameter measured by automated granulometry and manual analysis.

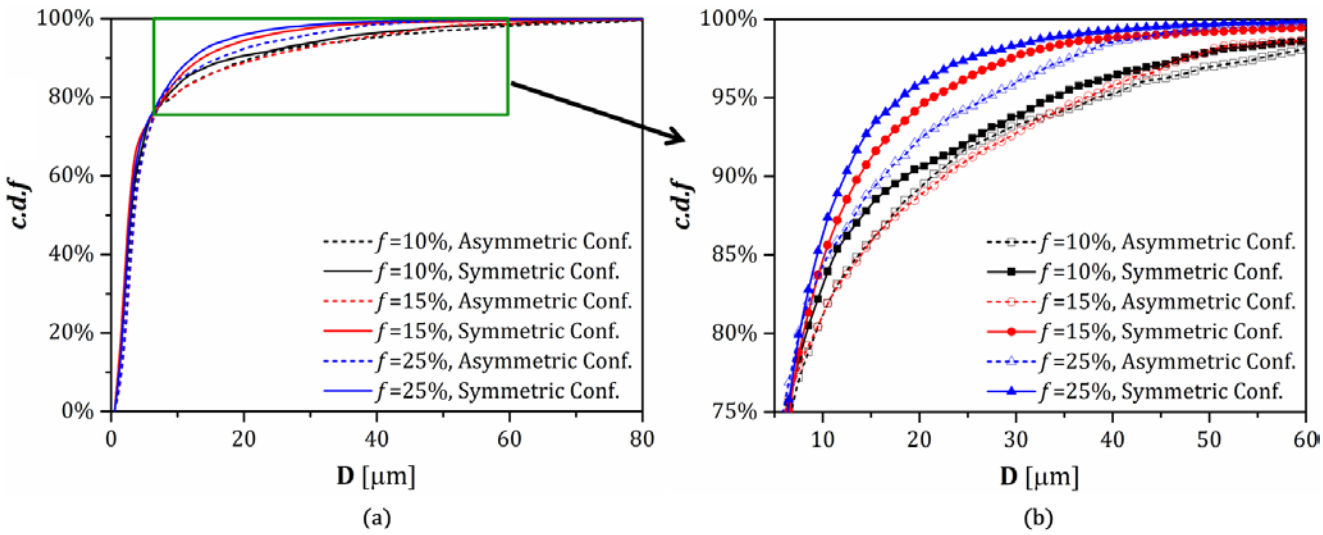

Fig.6. Cumulative distribution function of droplet diameter at Re_c=1524: (a)[0-80 μm]; (b)[5-60 μm].

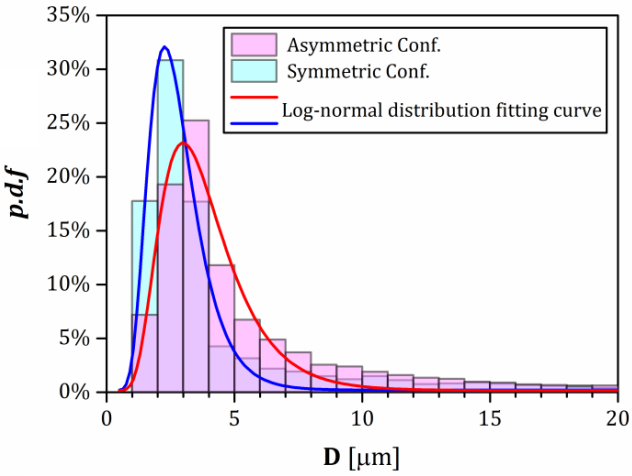

Fig.7. Probability distribution function of droplet diameter for two configurations at Re_c=1524 and f=10%.

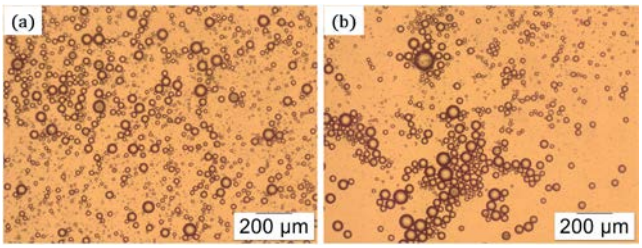

Fig.8. Microscopy images of emulsion sample for two configurations (a:symmetric configuration; b:asymmetric configuration) at Re_c=1524 and f=10%.

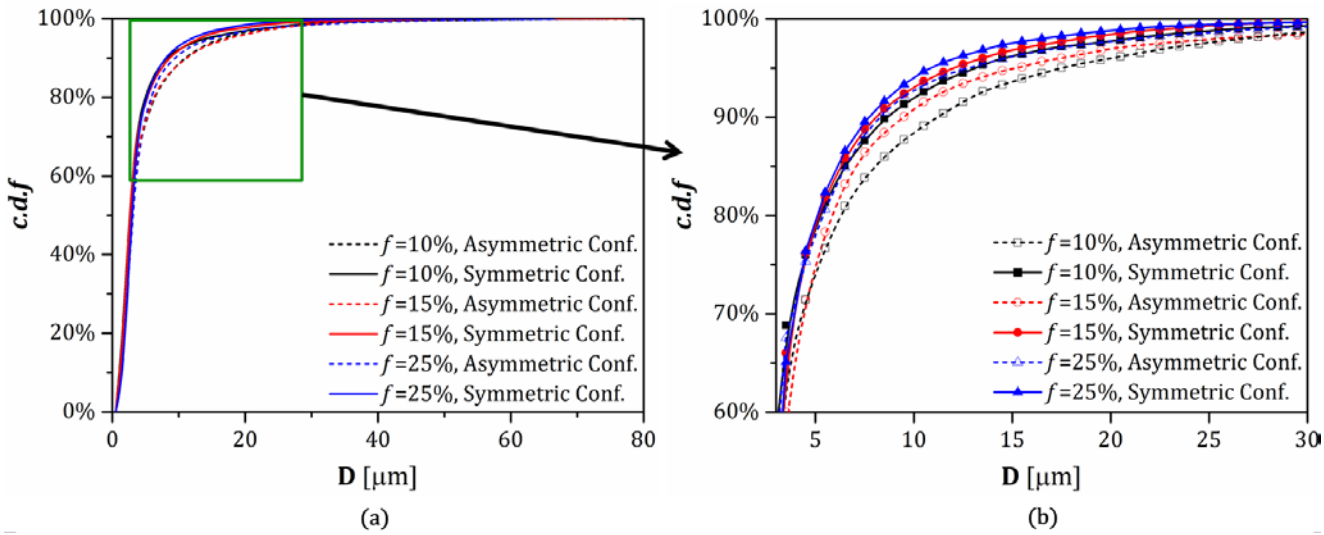

Fig.9. Cumulative distribution function of droplet diameter at Re_c=3047: (a)[0-80 μm]; (b)[3-30 μm].

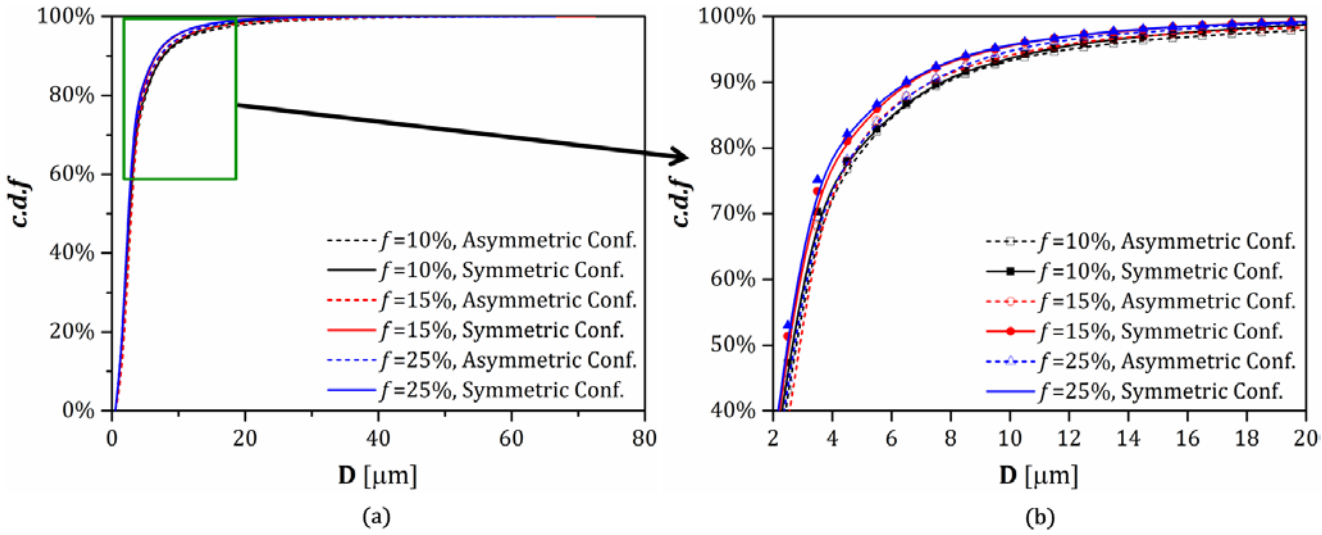

Fig.10. Cumulative distribution function of droplet diameter at Re_c=4570: (a)[0-80 μm]; (b)[5-60 μm].

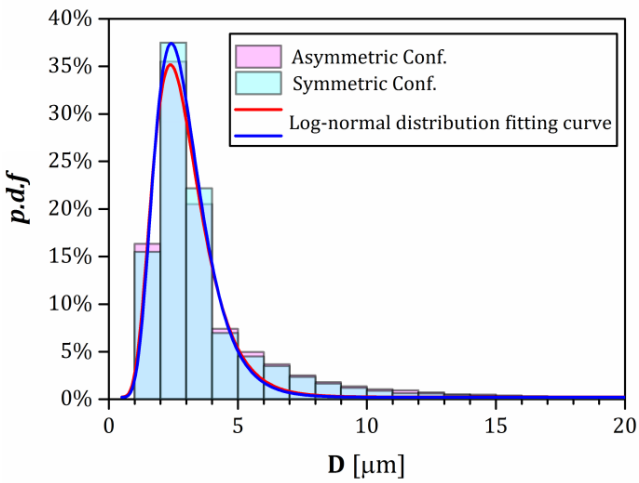

Fig.11. Probability distribution function of droplet diameter for two configurations at Re_c=4570 and f=10%.

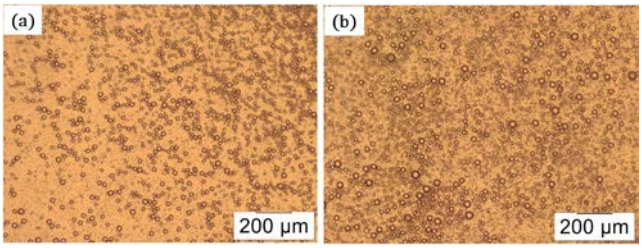

Fig.12. Microscopy images of emulsion sample for two configurations (a: symmetric configuration; b: asymmetric configuration) at Re_c=4570 and f=10%.

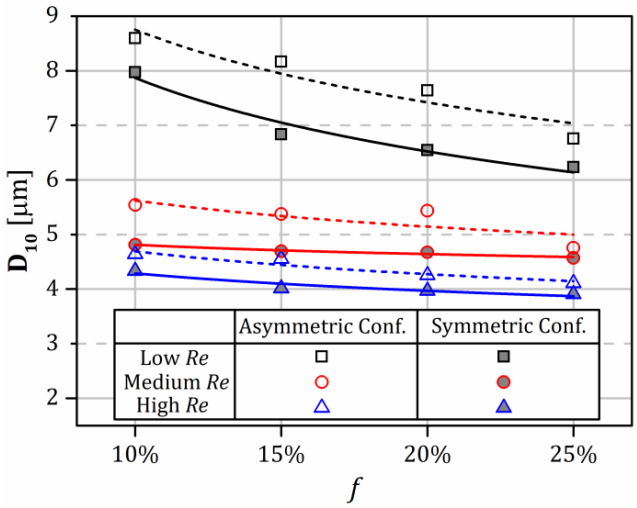

Fig.13. Arithmetic mean drop diameter for all cases.

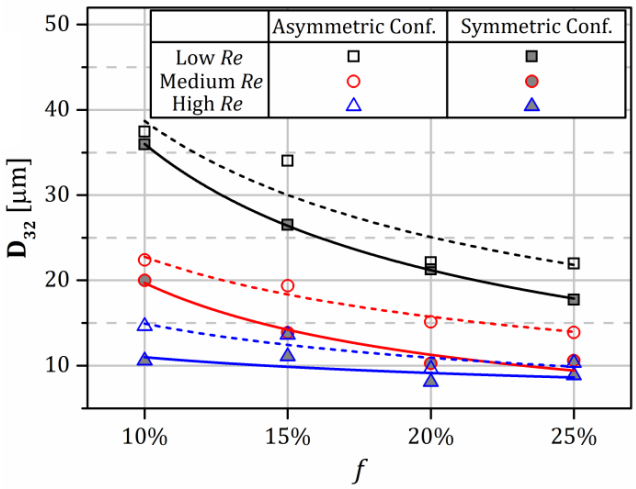

Fig.14. Sauter mean drop diameter for all cases.

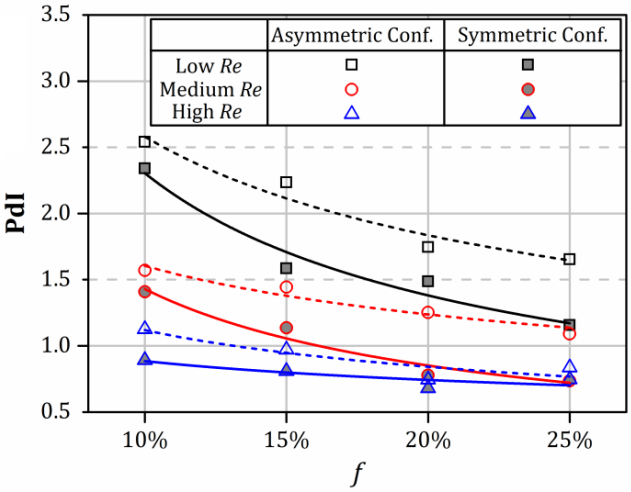

Fig.15. Polydispersity index for all cases.

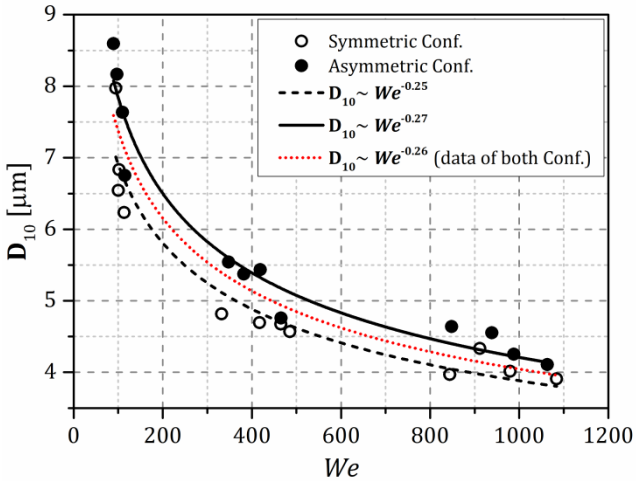

Fig.16. Correlation of arithmetic mean diameter with Weber number.

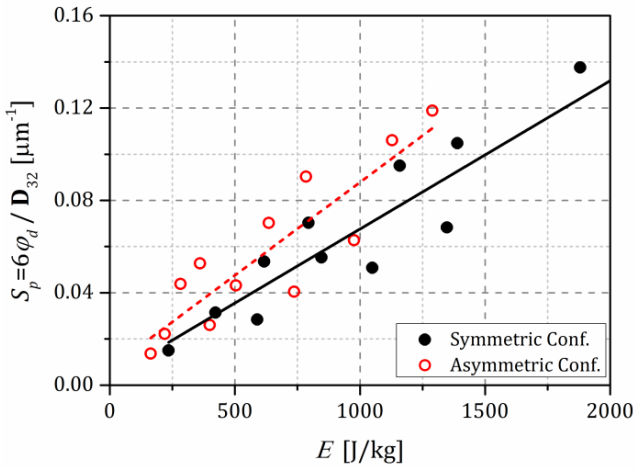

Fig.17. Variations of specific surface area with the energy cost.

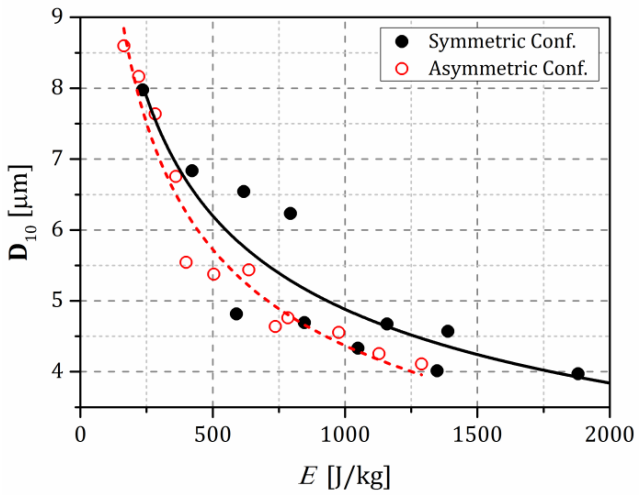

Fig.18. Variations of mean drop diameter with the energy cost.

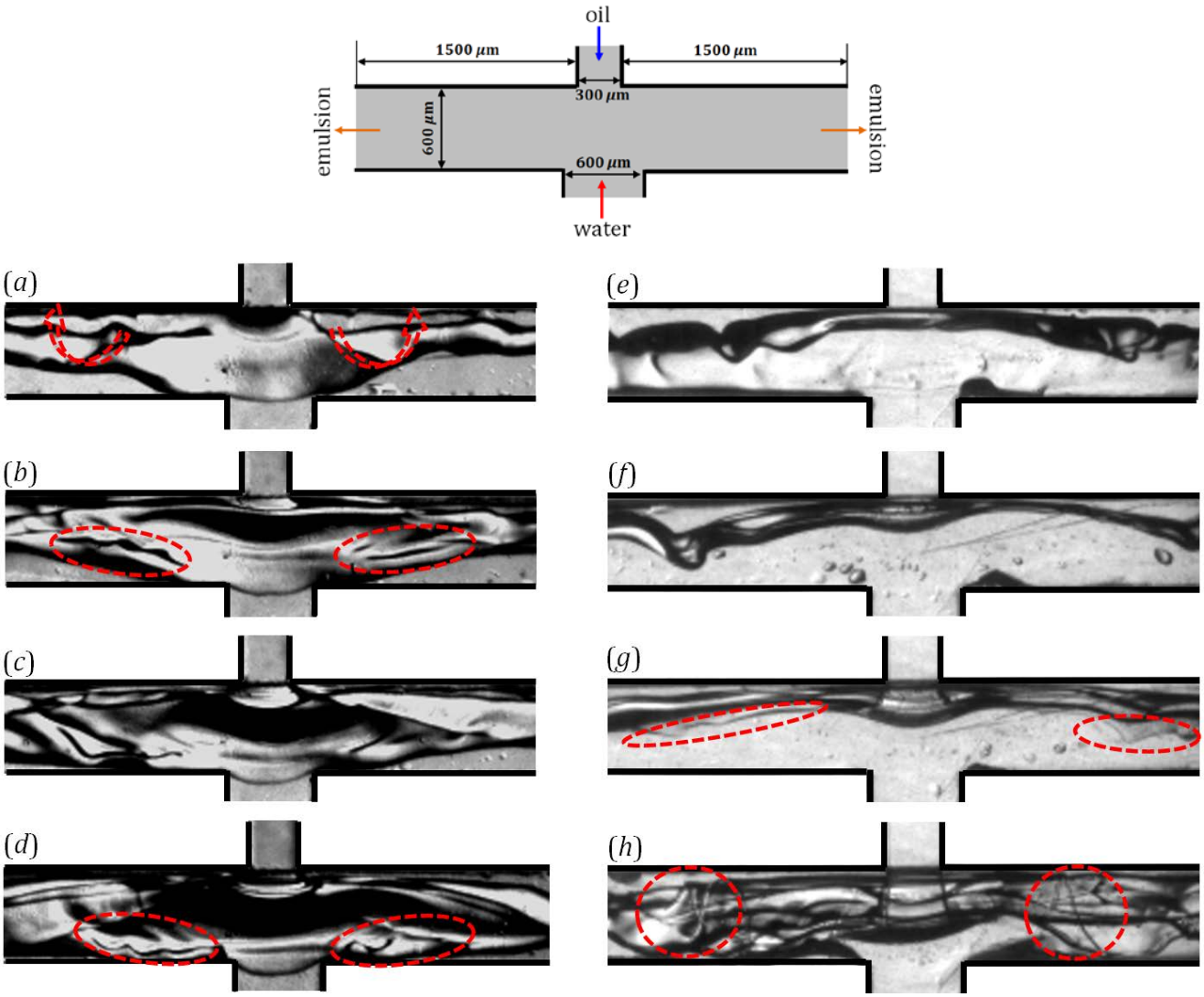

Fig.19. High-speed images of oil and water stream interactions at Re_c=1524: (a)-(d)asymmetric configuration with f varying as 10%, 15%, 20% and 25%; (e)-(h)symmetric configuration with f varying as 10%, 15%, 20% and 25%.

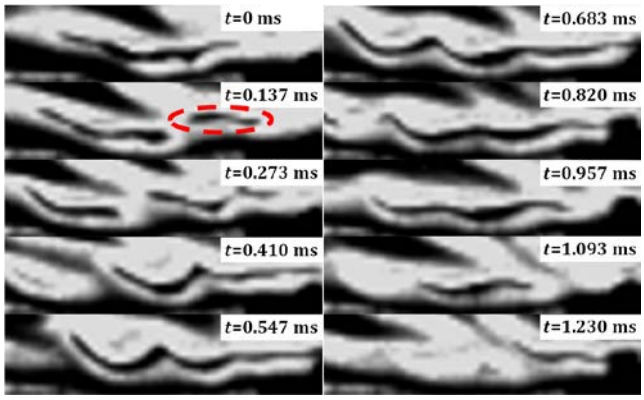

Fig.20. Evolution of filament instability in the asymmetric configuration at $Re_c = 1524$ and $f = 25\%$.

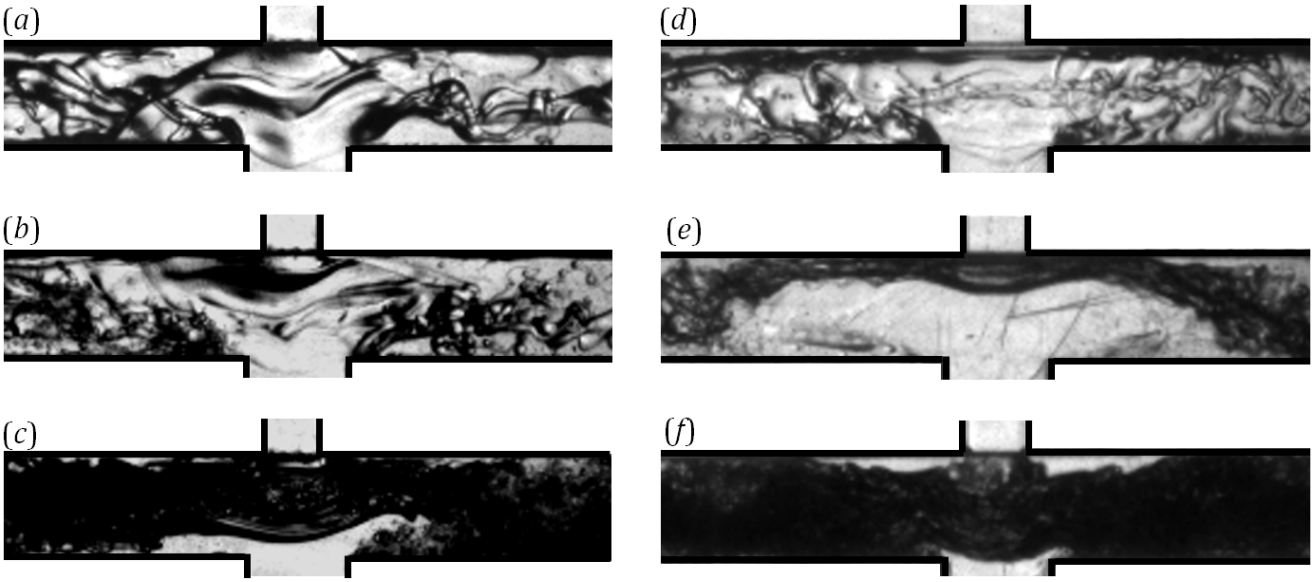

Fig.21. High speed images of oil and water stream interactions at medium and high Re conditions: (a)-(c)asymmetric configurations; (d)-(f)symmetric configurations; (a)&(d)$Re_c = 3047, f = 10\%$; (b)&(e)$Re_c = 4570, f = 10\%$; (c)&(f)$Re_c = 4570, f = 25\%$.